Chinese J. Chem. Eng., **13** (6) 776 – 782 (2005)

Effect of Chloride on the Atmospheric Corrosion of Cast Iron in Sulphur or Nitrogen-Bearing Pollutant Environment*

CAO Xia(曹霞) and XU Chunchun(许淳淳)**
Materials Science Department, Beijing University of Chemical Technology, Beijing 100029, China

Abstract The effect of chloride on the atmospheric corrosion of cast iron in sulphur or nitrogen-bearing pollutant was investigated by using periodic wet-dry test, electrochemical experiment and surface tension test. Scanning electron microscopy coupled with energy dispersive atomic (EDAX) and stereoscopic microscopy was used to identify the corrosion processes and products. Cl^- and NO_3^- were shown accelerating effects during the whole corrosion process but depression effects were observed in Cl^- and HSO_3^- bearing pollutant at the initial corrosion stage. However, with the corrosion going on, the depression effects was less obviously and the initial corrosion process was investigated from the viewpoint of surface activity. At the initial corrosion stage, the corrosion rate was proportional to the adsorptivity of anions, but as corrosion went on, the penetration effect of anions and different characteristics of the corrosion products began to dominate the corrosion process, which led to changes on the corrosion rate.
Keywords corrosion, simulated archaeological iron, corrosion rate, chloride, sulphur-bearing pollutant, nitrogen-bearing pollutant

1 INTRODUCTION

The effects of air pollutants and climatic parameters on the atmospheric corrosion of metal and its simulation have been the topics of several fields and laboratory studies. It is generally agreed that besides humidity and wetness time, deposition of sulfur dioxide, nitrogen dioxide and Cl^- as well as the pH value of rainfall are major factors determining the corrosion rate of metal. Many studies have focused on the synergism between two of the pollutants[1–3]. It has been found, for example, that at high relative humidity, aluminum and iron do not show SO_2+NO_2 synergism[4], and that for steel is negligible[5]. For metals with a protecting oxide film, NO_2 may even act as an inhibitor; otherwise, there seems to be synergistic effects[4]. In some investigations[6], synergistic effects of simultaneous interaction of SO_2+Cl^- with carbon steel have been observed. However, few studies were reported about the effect of chloride on the whole atmospheric corrosion process of cast iron in sulphur or nitrogen-bearing pollutant with grey cast iron simulating iron artifacts.

In the present study, corrosion behavior of simulated archaeological iron in NO_3^-, HSO_3^-, Cl^-+NO_3^-, and Cl^-+HSO_3^- bearing pollutants are comparatively investigated by means of mass loss measurement, electrochemical measurement and surface tension test as well as other analytical techniques. The main purpose is to study the effects of chloride on atmospheric corrosion of cast iron in sulphur or nitrogen-bearing pollutant with grey cast iron simulating iron artifacts.

2 EXPERIMENTAL

2.1 Preparation of specimen

The specimens used were grey cast iron to simulate cast iron artifacts, so the corrosion process would be in some ways similar to that observed in the field. Table 1 lists the chemical composition of cast iron simulating archaeological iron. The specimens were sectioned into 70 mm by 30 mm by 2 mm. They were grinded with 150-grit silicon carbide paper and finished with 600-grit paper. Then the specimens were ultrasonically washed in acetone and methanol, quickly dried and kept in a nitrogen atmosphere prior to the test.

Table 1 The chemical composition of cast iron simulating archaeological iron (%)

C	Si	S	P	Mn	Fe
3.00	1.84	0.089	0.097	0.083	rest

2.2 Interfacial tension test

Interfacial tension test was accomplished by a video frequency optical contact angle measurer (OCAZO). The effects of the anions on the interfacial tension were determined by measuring the respective contact angles of their solutions on the cast iron. To make the macro size solution droplet, 10—100 μl solution was put on to the metal using a suitable micro-syringe. Macro size droplets with the diameter of 0.5—5 mm salt solutions were placed onto a metal specimen. Then the edge and the region around it were observed carefully by a laser microscope. Wave length of the laser was 632.8 nm for this experiment.

2.3 Periodic wet-dry test

The periodic wet-dry test was performed in 0.01 mol·L^{-1} $NaNO_3$, 0.01 mol·L^{-1} $NaNO_3$+0.002 mol·L^{-1} NaCl and 0.01 mol·L^{-1} $NaHSO_3$, 0.01 mol·L^{-1} $NaHSO_3$+0.002 mol·L^{-1} NaCl solutions of pH=5 respectively in 1 L flasks at 35℃, which consisted of alternating wet periods of 10 min (in solution) and dry periods of 50 min (ambient tem-

Received 2005-01-21, accepted 2005-06-24.
* Supported by the National Key Technologies R&D Program of the Tenth 5-year Plan Period (No. 2001BA805B01).
** To whom correspondence should be addressed. E-mail: wangkaiti@126.com

perature). The corrosion rate was calculated by mass loss at periods of 24, 48, 72 and 84 cycles. Three specimens were taken out each time and rinsed with distilled water, degreased and scrubbed with cotton balls to remove the corrosion products. The remainder of the corrosion products was immersed in 50% H_2SO_4 at ambient temperature. In the end specimens were dried in oven at 80℃ for one hour and weighed to within 0.1 mg.

2.4 Electrochemical polarization test

Electrochemical polarization tests were accomplished by using a Corrtest instrument. The potentiostat was programmed to apply a continuously varying potential to the sample from −0.5 to 0.5 V. All potentials were measured versus the open circuit potential. Polarization curves were produced in 0.01 mol·L^{-1} $NaNO_3$ aqueous solution, 0.01 mol·L^{-1} $NaNO_3$+0.002 mol·L^{-1} NaCl aqueous solution and 0.01 mol·L^{-1} $NaHSO_3$ aqueous solution, 0.01 mol·L^{-1} $NaHSO_3$+0.002 mol·L^{-1} NaCl aqueous solution respectively at a sweep rate of 0.5 mV·s^{-1} after stabilization of the open circuit potential.

Electrochemical impedance measurements were performed to evaluate the protection performance of the corrosion products formed after the periodic wet-dry test. An M398 corrosion measurement system manufactured by EG&G was used to undertake electrochemical impedance (EIS) measurements. A Princeton flat cell three-electrode system was selected in which the reference electrode was a saturated calomel electrode (SCE), and the counter electrode was a platinum foil. The 10 mm×10 mm exposed area of specimens was prepared as described above, and other surfaces were shielded with epoxy. A sine wave amplitude of 10mV and a frequency range of 100 kHz—10 MHz were used.

2.5 Analysis methods

Corrosion products on the rusted specimen were examined by scanning electron microscopy (SEM). SEM observations were made by using a Philips 515 microscope, which was coupled with a 9100 energy dispersive Atomic (EDAX) for surface analysis. SEM and EDAX data were used to characterize the morphology and chemical heterogeneities of corrosion products.

3 RESULTS AND DISCUSSION

3.1 Surface tension test

The ion adsorption at the interface between electrode and solution has significant effects on the kinetics of electrode processes. Different ion has different adsorption ability and most inorganic anions are obedient to typical ion adsorption rules because most anions are surfactants. The adsorption of anions can not only change the electrode surface states and double layer distribution, but also affect both the concentration of reactants and the activation energy on the electrode. Thus the reaction rate would vary even though the anions themselves do not take part in any reaction. Of course the reaction kinetics will be directly affected if these ions participate in the reactions. The surface tension and adsorption ability can be quantified and compared by measuring the respective contact angles. Photos of the macro-size droplets placed on the metal specimen were shown in Fig. 1. Contact angles of the three solutions on the iron specimen were shown in Table 2. From these data, we can judge easily that the adsorption inclination on cast iron electrode is 0.01 mol·L^{-1} $NaHSO_3$ > 0.01 mol·L^{-1} $NaHSO_3$+0.002 mol·L^{-1} NaCl, 0.01 mol·L^{-1} $NaNO_3$+0.002 mol·L^{-1} NaCl> 0.01 mol·L^{-1} $NaNO_3$. The stronger the absorption ability of the anion is, the more probability it will have to attack the metal at the initial corrosion stage.

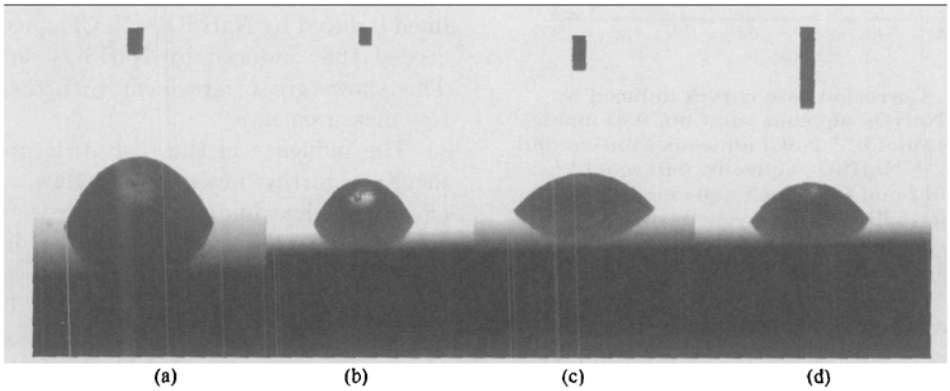

Figure 1 Pictures of micro-droplets on the cast iron
(a) $NaNO_3$; (b) $NaNO_3$+NaCl; (c) $NaHSO_3$; (d) $NaHSO_3$+NaCl

Table 2 Contact angles of the drop on solution/iron interface

0.01 mol·L^{-1} $NaNO_3$	0.01 mol·L^{-1} $NaNO_3$+ 0.002 mol·L^{-1} NaCl	0.01 mol·L^{-1} $NaHSO_3$	0.01 mol·L^{-1} $NaHSO_3$+ 0.002 mol·L^{-1} NaCl
50°	42°	29°	36°

3.2 Mass loss measurement

Corrosion rates of the cast iron simulated iron artifacts were determined by using mass loss measurement. Corrosion rates were only recorded when the specimen had already been uniformly corroded. Variation of the corrosion rate induced by 0.002 mol·L^{-1} NaCl+0.01 mol·L^{-1} $NaNO_3$, 0.01 mol·L^{-1} $NaNO_3$, 0.01 mol·L^{-1} $NaHSO_3$+0.002 mol·L^{-1} NaCl and 0.01 mol·L^{-1} $NaHSO_3$ solution of pH=5 during periodic wet-dry tests is shown in Fig. 2. It was clearly observed that the corrosion rates were all high during the initial stage of the test and dropped notably as time elapsed. The differences between the corrosion rates at the early corrosion stage were obvious. However, as time advanced, the corrosion rate dropped and the differences were less significant. Corrosion rate of specimen induced by NaCl+$NaNO_3$ solution was much higher than that induced by $NaNO_3$ solution, and dropped more slowly at the later period. However, the corrosion rate of specimen induced by $NaHSO_3$+NaCl solution was much lower than that induced by $NaHSO_3$ solution at the initial stage and dropped more slowly as corrosion progressed. This is contrast to that induced by $NaHSO_3$ solution which dropped sharply. At the late period, the corrosion rate induced by $NaHSO_3$+NaCl was close to that induced by $NaHSO_3$.

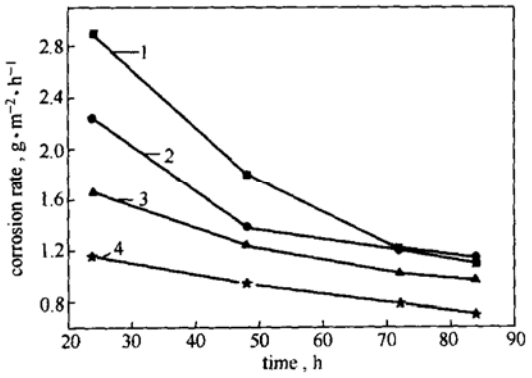

Figure 2 Corrosion rate curves induced by 0.01 mol·L^{-1} $NaNO_3$ aqueous solution, 0.01 mol·L^{-1} $NaNO_3$+0.002 mol·L^{-1} NaCl aqueous solution and 0.01 mol·L^{-1} $NaHSO_3$ aqueous, 0.01 mol·L^{-1} $NaHSO_3$+0.002 mol·L^{-1} NaCl aqueous solution in periodic wet-dry-cyclic test
1—$NaHSO_3$; 2—$NaHSO_3$+NaCl; 3—$NaNO_3$+NaCl; 4—$NaNO_3$

It can be concluded that when Cl^- is present in $NaNO_3$ bearing pollutant, the attack to iron is accelerated and accelerated effect is obvious; when Cl^- is present in $NaHSO_3$ bearing pollutant, the attack to iron is inhibited at the initial corrosion stage. And it is less inhibited with the corrosion proceeding. The law of corrosion rate at the initial stage shows great agreement with the adsorption ability of anions contained in the solution. The higher the absorption ability the anion has, the heavier its attack on the metal is. The different characteristics of the corrosion products and the different penetration ability of anions may be the two key factors that affect the corrosion rate at the later stage, whereas the radius of chloride is very small. When Cl^- exists in NO_3^- and HSO_3^- bearing environment, its high penetration ability would cause heavy attack on iron in spite of the thickness of the rust layers.

3.3 Electrochemical test

Figure 3(a) illustrates the potentiodynamic polarization curves of bared specimens in 0.01 mol·L^{-1} $NaNO_3$ aqueous solution, 0.01 mol·L^{-1} $NaNO_3$+0.002 mol·L^{-1} NaCl aqueous solution of pH=5, and Fig. 3(b) shows the Potentiodynamic polarization curves of bare specimens in 0.01 mol·L^{-1} $NaHSO_3$+0.002 mol·L^{-1} NaCl aqueous solution and 0.01 mol·L^{-1} $NaHSO_3$ aqueous solution of pH=5. It is worth noting that there was little difference in corrosion rates from the mass loss measurements. It was likely that there was not enough time to form a protective layer on the specimen surface because the polarization test was made very rapidly.

As can be seen from Figs. 3(a) and (b), when NaCl was added into $NaNO_3$ aqueous solution, the open circuit potential decreased. Anodic current density increased remarkably along with the increasing applied anodic potential. Corrosion current of specimen induced by NaCl+$NaNO_3$ aqueous solution was much higher than that induced by $NaNO_3$ aqueous solution at the same potential. This is accordant with the result of mass loss measurement at the initial stage and the result of surface tension tests. When NaCl was added into $NaHSO_3$ aqueous solution, the open circuit potential increased. The corrosion current of specimen induced by $NaHSO_3$+NaCl aqueous solution was much lower than that induced by $NaHSO_3$ aqueous solution below −0.63 V. However, when the applied potential increased, corrosion current of specimen induced by $NaHSO_3$+NaCl aqueous solution exceeded that induced by $NaHSO_3$ aqueous solution. This shows great agreement with the result of mass loss measurements.

The influence of the rust structure on the specimens was further investigated by measurements of the electrochemical impedance. In order to evaluate the protection performance of the rust, impedance measurement of various rusted specimen was carried out in 0.01 mol·L^{-1} NaCl aqueous solution. The EIS data are showed in Figs. 4 and 5. It can be seen in Fig. 4 that the two impedance spectrums have the same characteristics. Both low frequency parts of the impedance show the feature of Warburg impedance. Here the system was affected by concentration relaxation, the phase angle of the diffusion tail deviates from 45 degree. Compared with that induced by NaCl+$NaNO_3$ aqueous solution, the Warburg impedance value of the rust layer induced by $NaNO_3$ is obviously higher,

which shows stronger inhibition effect on the transfer of corrosion medium to the electrode surface, thus the protection for the metal substrate is better.

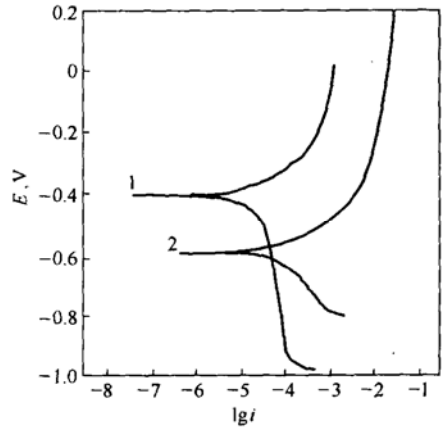

(a) 1—$NaNO_3$; 2—$NaNO_3$+NaCl

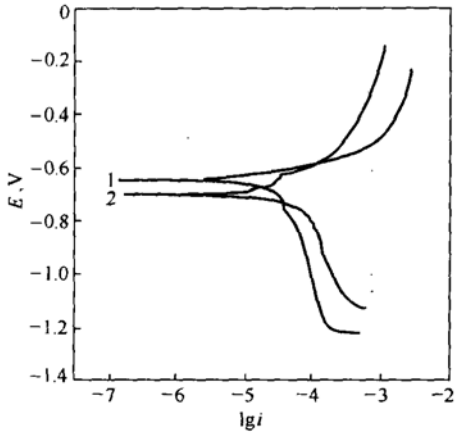

(b) 1—$NaNSO_3$+NaCl; 2—$NaHSO_3$

Figure 3 Polarization curves of bare iron in (a) 0.01 mol·L^{-1} $NaNO_3$ aqueous solution, 0.01 mol·L^{-1} $NaNO_3$+0.002 mol·L^{-1} NaCl aqueous solution and in (b) 0.01 mol·L^{-1} $NaHSO_3$ aqueous solution, 0.01 mol·L^{-1} $NaHSO_3$+0.002 mol·L^{-1} NaCl aqueous solution solutions of pH=5

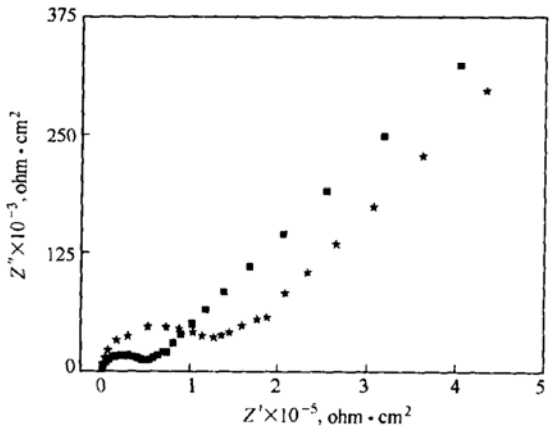

Figure 4 EIS for the rusted specimen induced by $NaNO_3$ and $NaNO_3$+NaCl
■ $NaNO_3$+NaCl; ★ $NaNO_3$

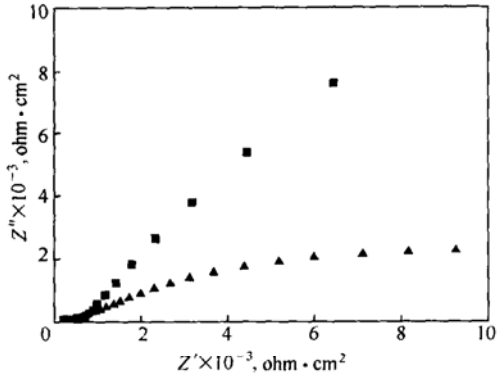

Figure 5 EIS for the rusted specimen induced by $NaHSO_3$ and $NaHSO_3$+NaCl
■ $NaHSO_3$; ▲ $NaHSO_3$+NaCl

EIS of the rusted specimen induced by $NaHSO_3$ aqueous solution has different characteristics. Its low frequency(LF) part transits from a semi-circle to a line whose slant angle is 45°. This feature manifests the control of concentration polarization. The tiny arc presented within the high frequency part of the capacitance reactance curve manifests that the rusted layer formed on the specimen surface has kept corrosion medium from reaching the metal substrate. The corrosion products have some protection effects on the metal base.

In the solution containing both NaCl and $NaHSO_3$, the EIS is a single capacitance reactance arc belonging to a caked circle of big radius. The caked semicircle shows that the surface double layer has deviated from ideal capacitor and the polyphase and complex structure of the surface has resulted in diffusion phenomenon.

3.4 Surface analysis

Generally speaking, rusts have important effects on the subsequent corrosion rate. The rusted specimen were kept in 100% RH and studied under microscopy to compare their micro-morphology after 72 cycles. As shown in Figs. 6(b, d), weeping [7] (other descriptive terms "yellow beads of liquid or brown globules of liquid") is observed clearly, which may be due to the presence of Cl^-. The same phenomena do not appear in the specimens immersed in $NaNO_3$ and $NaHSO_3$ solutions as shown in Figs. 6 (a, c). Fig. 6(a) exhibits a uniform and compact corrosion layer. In contrast, Figs. 6(b, c, d) demonstrated a more severe attack on the rust layer.

To analyze the effects of the rust layer, SEM coupled with EDAX analysis patterns were used for identifying the constituents of rust layer formed on the specimens just after 48 cycles. SEM and EDAX analysis on the samples after period test in four different solutions are shown in Figs. (7)—(10).

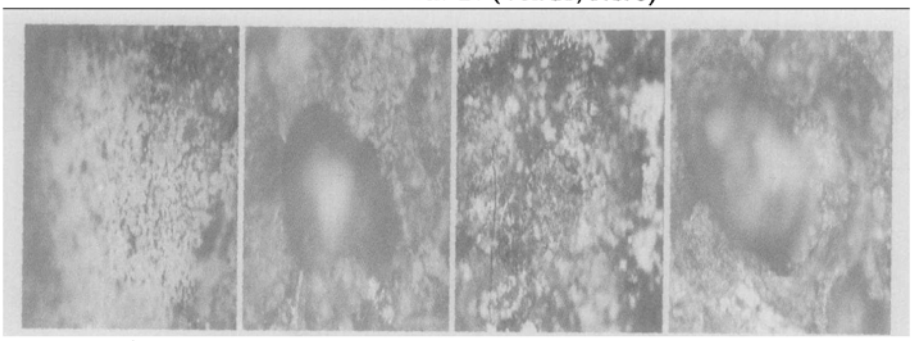

Figure 6 Micrograph of the rust samples induced by: (a) NO_3^-, (b) NO_3^-+NaCl, (c) HSO_3^-, (d) HSO_3^-+NaCl

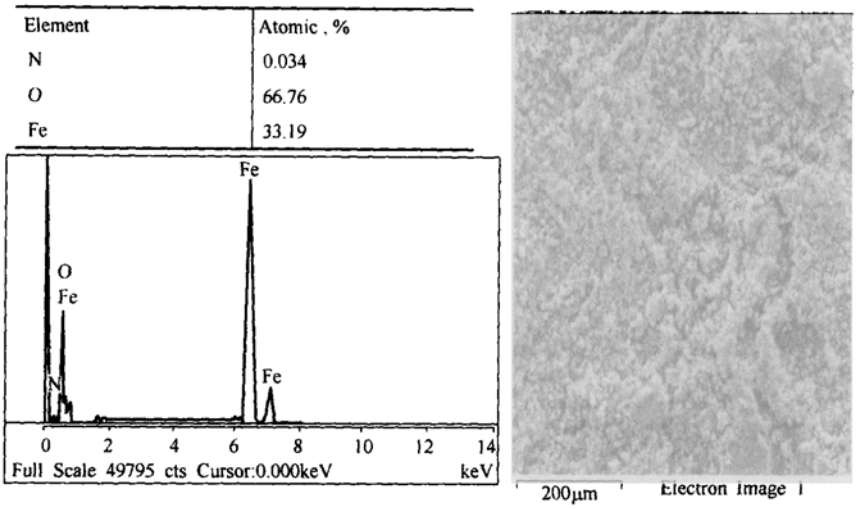

Figure 7 SEM micrographs and EDAX analysis of rusted sample induced by $NaNO_3$ after 48 cycles

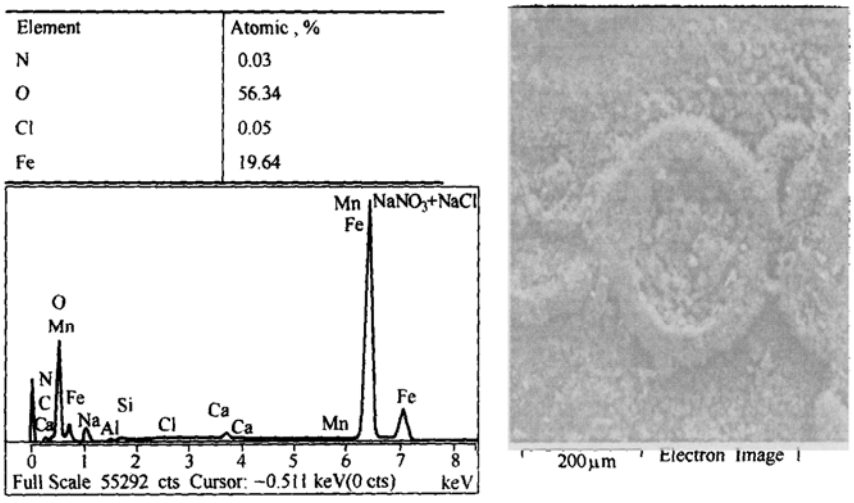

Figure 8 SEM micrographs and EDAX analysis of rusted sample induced by $NaNO_3$+NaCl after 48 cycles

SEM micrographs shows that attack on the specimen induced by $NaHSO_3$ environment is stronger than that induced by $NaNO_3$ environment as presented by the stereoscope. When Cl^- ions were present in the solution, the rusted layers of the specimen seemed to be much rougher than that induced by the other two monocomponent solutions. This was one of the reasons why the corrosion rate at the late periods was higher than that in the monocomponent solution.

There were wide pits as observed in Figs. 8 and 10. Cl was found in every pit. EDAX analysis on corrosion products shows that flat areas where uniform corrosion is observed in Fig. 7 contains lower content of O. The ratio of O to Fe in the corrosion product

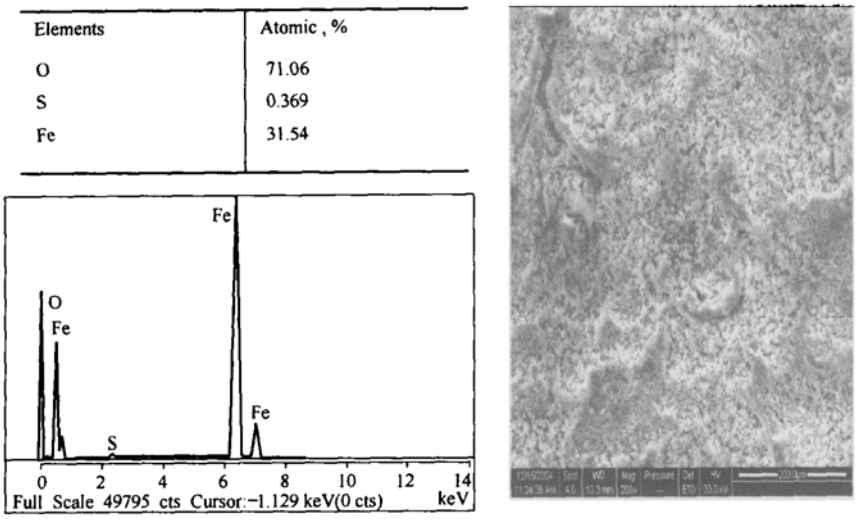

Figure 9 SEM micrographs and EDAX analysis of rusted sample induced by $NaHSO_3$ after 48 cycles

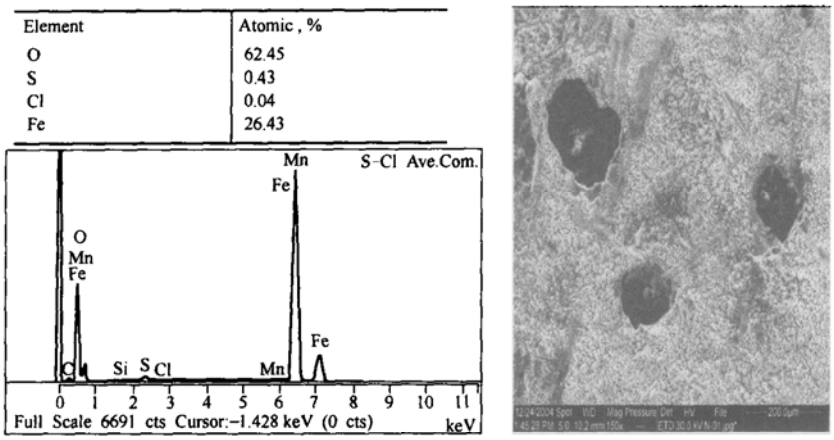

Figure 10 SEM micrographs and EDAX analysis of rusted sample induced by $NaHSO_3$+NaCl after 48 cycles

was nearly 2:1 in NO_3^- bearing environment. This might be attributed to the existence of a large mount of FeOOH. In other word more Fe^{3+} existed in the rust layer induced by $NaNO_3$. At the same time, minor constituent of "N" was present in the corrosion product which can be assigned to the soluble nitrate formed during the corrosion process. If chloride is present in $NaNO_3$ solution, the ratio of O to Fe in the product increases. Absolutely more Cl is found as Fig. 8 shown. This can be attributed to the formation of GR1[8] (green rust 1), whose formula is $3Fe(OH)_2 \cdot Fe(OH)_2Cl \cdot nH_2O$ which was insoluble. GR1 obtained in these conditions is unstable and can be oxidized to lepidocrocite (γ-FeOOH) by rapid aerial oxidation and magnetite (Fe_3O_4) by slow aerial oxidation[9]. In Figs. 9 and 10, higher ratios of O to Fe were also observed, which are 3.4:1 and 2.5:1, respectively. A great deal of "S" is found in Fig. 10 and a great deal of "S" together with a minor of "Cl" is found in Fig. 11. This should be attributed to the generation of such resultants as $FeSO_4 \cdot nH_2O$ or GR1. That is to say that the high ratio of O to Fe demonstrates the existence of Fe^{2+}.

The micro-morphology and the constituent of the corrosion products revealed good agreement with the corrosion rates at the late corrosion stage estimated from the mass loss measurements and the electrochemical tests. Cl^- ions contribute to the corrosion with the corrosion processing.

As an active oxidizer, HNO_3 produced during the corrosion process can oxidize Fe and Fe^{2+} to Fe^{3+}, which inhibits the formation of Fe^{2+} state. O_2 reduction reaction is more inclined to take place where the mount of Fe^{2+} is high, so the concentration of Fe^{2+} ions at the outmost part of the oxide surface could determine the kinetics of the O_2 reduction[10]. Besides this, good protection performance of the rust layer induced by NO_3^- as shown in Fig. 4 and the poor penetration ability of NO_3^- ion were other reasons why the corrosion rate of iron in NO_3^- bearing pollutants was the lowest.

However when Cl^- is present in NO_3^- bearing pol-

lutants, the surface tension decreases. More NO_3^- ions together with Cl^- ions are adsorbed on the surface of electrode. Corrosion rate is accelerated at the initial corrosion stage. Meanwhile more Fe^{2+} is produced during the corrosion process which also promotes the dissolution of cast iron. It had been reported[11] that Cl^- inhibits the phase transformation from γ-FeOOH to the more stable α-FeOOH. With the corrosion going on, the poor protection performance of the rusted layer as Fig. 4 presented and the high mobility of Cl^- also accelerates the corrosion process.

The corrosion mechanisms for iron corrosion in the presence of sulfite and chloride are similar. The whole corrosion process proceeds according to "the acid regeneration cycle mechanism". However, there are still many differences during the process. Compared with Cl^- ions, the effect of HSO_3^- on the iron corrosion is stronger at the initial stage, which is related to its even higher surface activity. Meanwhile SO_2 is generated during the corrosion reaction, which can substitute for oxygen to participate in the corrosion process as a depolarizer. This can contribute to the anodic dissolution and cause the generation of $FeSO_4 \cdot 7H_2O$, $FeSO_4 \cdot 9H_2O$ and γ-FeOOH whose protection for the substrate were weak[12]. As seen from Figs. 6(c) and 9, the rust layer is rough.

When Cl^- is present in HSO_3^- bearing pollutant, concentration of HSO_3^- ions on the surface of electrode absolutely decreases. For one reason the adsorption ability of solution decreased and for another reason competitive adsorption occurred. Meanwhile the effect of Cl^- ion on the corrosion of the specimen is weaker than that of HSO_3^- ions at the initial stage, so the corrosion rate induced by $Cl^- + HSO_3^-$ is much lower than that induced in $NaHSO_3$ at the initial time. However, as presented above, Cl^- can inhibit the phase transformation from γ-FeOOH to α-FeOOH, which makes the protection performance of rust layer even weaker. Taking note of the penetration effect of Cl^-, it can be understood that the corrosion rate in the multicomponent was higher than that in monocomponent solution of $NaHSO_3$ at the late stage when minor Cl^- ions were present in $NaHSO_3$ environment.

4 CONCLUSIONS

(1) The attack of anions to the metal at initial corrosion stage show great agreement with their surface activity. However, as corrosion went on, the penetration effect of anions together with the different characteristics of the corrosion products came to control the corrosion process.

(2) When minor Cl^- was present in NO_3^- aqueous solution, iron shows accelerated corrosion which was chiefly due to the increase of surface activity at the initial corrosion stage and the penetration effect of Cl^- at the late corrosion periods.

(3) When minor Cl^- was present in of HSO_3^-, Corrosion rate was inhibited at the initial corrosion stage which was due to the decrease of surface activity and was less inhibited at the late corrosion stage which was mainly due to the penetration effect of Cl^-.

NOMENCLATURE

E	electric potential, V
i	current density, $A \cdot cm^{-2}$
RH	relative humidity
Z'	real resistance impedance, $ohm \cdot cm^2$
Z''	imaginative resistance impedance, $ohm \cdot cm^2$

REFERENCES

1 Juan, J., Santana, Rodriyuez, "The effect of environmental and meteorological variables on atmospheric corrosion of carbon steel, copper, zinc and aluminum in a limited geographic zone with different types of environment", *Corrosion Science*, **45**, 799—815 (2003).

2 Oesch, S., Faller, M., "Environmental effects on materials: The effect of the air pollutants SO_2, $NO_2 \cdot NO$ and O_3 on the corrosion of copper, zinc and aluminum", *Corrosion Science*, **39** (9), 1505—1530 (1991).

3 Pyan, S.J., "Effects of Cl^-, NO_3^- and SO_4^{2-} ions on anodic dissolution of pure aluminum in alkaline", *Corrosion Science*, **41**, 653—667 (1999).

4 Oesch, S., Faller, M., "The effect of on the corrosion of unalloued carbon steel an weathering steel—The results of laboratory exposure", *Corrosion Science*, **38** (8), 1357—1368 (1996).

5 Kuccera, V., "Dose-response relations from the un ece project as a tool for air pollution abatement strategics", 13th International Corrosion Congress, Melbourne, Australia (1996).

6 Cai, J.P., "Synergistic effect of chloride and sulphur-bearing pollutant in atmospheric corrosion of mild steel", *Journal of Chinese for Corrosion and Protection*, **16** (4), 303—306 (1996).

7 Cronyn, J.M., The Elements of Archaeological Conservation, Routledge, London, 194—195 (1990).

8 Re, P.H., Fai, T., "The oxidation of ferrous hydroxide in chloride containing aqueous media and pourbaix diagram of green rust one", *Corrosion Science*, **34** (5), 797—819 (1993).

9 Askey, A., BLyon, S., "The corrosion of iron/and zinc by atmospheric hydrogen chloride", *Corrosion Science*, **25**, 379—391 (1990).

10 Misawa, T., "The mechanism of formation of iron oxide and oxyhydroxides in aqueous solutions at room temperature", *Corrosion Science*, **14**, 131—149 (1974).

11 Zhang, A.F., "Factors that effect the atmospheric corrosion of steel and iron", *Material Protection*, **22** (2), 15 (1989).

12 Han, W., Jia, W., "Effect of SO_2 on corrosion mechanism of A3 steel at dewing environment", *Journal of Chinese for Corrosion and Protection*, **22** (6), 355—358 (2002).